Pergamon

Int. J. Heat Mass Transfer. Vol. 38, No. 1, pp. 91–100, 1995

0017-9310/95 $9.50+0.00

0017-9310(94)00135-9

Laser holographic interferometry study of developing heat transfer in a duct with a detached rib array

TONG-MIIN LIOU and WEN-BIN WANG

Department of Power Mechanical Engineering, National Tsing Hua University, Hsinchu, Taiwan 30043, R.O.C.

(*Received* 24 *December* 1993 *and in final form* 11 *April* 1994)

Abstract—Laser holographic interferometry measurements of temperature distributions are presented for a developing rectangular duct with a detached square-rib array and an abrupt-contraction inlet. The Reynolds number based on the duct hydraulic diameter and bulk mean velocity extended from 5.0×10^3 to 5.0×10^4. The ratios of rib pitch to height, rib to duct height, and detached distance to rib height were 10, 0.13 and 0.58, respectively. Isotherm contours and local and average Nusselt number distributions were used to document the heat transfer characteristics. The complementary pressure loss measurements allowed thermal performance comparison between detached-ribbed, attached-ribbed and smooth ducts to be made. It was found that thermal performance was better in the detached-ribbed duct flows than in the attached-ribbed duct flows. The entry length effect was 5.3–10.6% in terms of length–mean Nusselt number ratio for the detached-ribbed duct flows. Further, semi-empirical correlations for heat transfer and friction in the fully developed region and length mean Nusselt number ratio were developed.

INTRODUCTION

In heat exchange systems ducts with rib elements are often used to enhance forced convection heat transfer [1–5]. Previous heat transfer [4] and fluid flow [6] studies indicated that for the solid ribs attached on the walls, the heat transfer locally deteriorated immedi-ately behind the ribs. To eliminate or alleviate the local heat transfer deterioration in the rear concave corners of the attached solid ribs, heat transfer measurements in a channel with perforated ribs mounted on the walls have been performed [7] and the results showed that perforated ribs could remove the aforementioned heat transfer deterioration. As a possible alternative to the perforated ribs for manufacturing concern, the detached solid ribs positioned at a small distance from one wall are adopted in the present work.

Fujita *et al.* [8] investigated forced convection heat transfer on a flat plate with zero pressure gradient in which a single circular cylinder was inserted normal to the free stream direction and positioned at a clearance from the plate. They found that heat transfer enhancement could be achieved with a suitable selection of the clearance. Kawaguchi *et al.* [9] investigated the heat transfer augmentation with a number of circular cylinders positioned in a line and attached to or near one wall at various streamwise pitches by measuring the heat transfer coefficient. They found that among the pitch to cylinder diameter ratios tested (6.25, 12.5, 25, 50, ∞), the values 12.5 and 25 are appropriate as far as overall heat transfer augmentation is concerned. Oyakawa *et al.* [10] studied how the heat transfer augmentation in the fully developed region is affected by the geometric shape (a straight band plate, an angled band plate and a T band plate) and clearance of the turbulence promoters which are set in a staggered arrangement near two opposite walls of a rectangular duct. The roles of the Karman vortex shedding and reattachment were documented in detail. Some shapes of turbulence promoters were found to provide a marked improvement in thermal performance as compared with the previously reported cylinder case. For duct flows with a staggered array of circular cylinders near two opposite walls, Yao *et al.* [11, 12] found that, after the first three cylinders, an almost fully developed state was attained thermally and hydrodynamically and that a more than three times larger averaged Nusselt number, relative to that in the smooth duct flow, can be achieved. Moreover, the measured distribution of the local Nusselt number was found to be similar in shape regardless of the Reynolds number ($8 \times 10^3 < Re < 6 \times 10^4$).

As far as the experimental techniques are concerned, hot-wire anemometers and flow visualization methods were respectively used to quantitatively and qualitatively characterize the flow field and thermocouples were used to measure the temperature distribution in the aforementioned works. The present paper intends to employ the non-intrusive laser holographic interferometry (LHI) for quantitative measurements of the local heat transfer coefficients in a ribbed duct. Moreover, for turbulent duct flows with a detached-rib array no data have been reported for square rectangular ribs. Laminar

NOMENCLATURE

A	duct half-width [m]
B	duct half-height [m]
C	clearance between rib and wall [m]
C_f	skin-friction coefficient, $2(P_X - P_0)/\rho U^2$
c_p	specific heat at constant pressure [$m^2 s^{-2} K^{-1}$]
D_e	hydraulic diameter, $4B/(1 + B/A)$ [m]
f	(Darcy) friction factor
H	rib height [m]
h	heat transfer coefficient [$W m^{-2} K^{-1}$]
k_f	air conductivity [$W m^{-1} K^{-1}$]
L_h	wetted length of heated surface in one pitch
m	mass flow rate [$kg s^{-1}$]
Nu	local Nusselt number
$\overline{Nu}$	average Nusselt number
$\overline{Nu}_m$	length mean Nusselt number
$\overline{Nu}_p$	periodic fully developed average Nusselt number for the ribbed duct
$\overline{Nu}_s$	average Nusselt number for the smooth duct (at the same mass flow rate)
$\overline{Nu}_s^*$	average Nusselt number for the smooth duct (at the same pumping power)
P	pressure [$N m^{-2}$]
Pi	rib pitch [m]
P_0	ambient pressure [$N m^{-2}$]
Pr	Prandtl number
P_X	static pressure of channel spanwise midpoint at axial station X [$N m^{-2}$]
Q	quantity of heat given to air from entrance to the considered cross-section of the duct [W]
q_{conv}	local convective heat transfer flux from the wall [$W m^{-2}$]
Re	Reynolds number
Re^*	Reynolds number for the smooth duct (at the same pumping power)
T	temperature of air [K]
T_b	local bulk mean temperature of air [K]
T_{in}	air temperature at duct inlet (i.e. room temperature) [K]
T_w	local wall temperature [K]
$\bar{T}_b$	average bulk mean temperature of air [K]
$\bar{T}_w$	average wall temperature [K]
U	axial mean velocity [$m s^{-1}$]
X	axial coordinate ($X = 0$ at inlet reference, Fig. 2) [m]
X_N	axial coordinate ($X = 0$ at rib real edge, Fig. 2) [m]
Y	transverse coordinate, Fig. 2 [m]
Z	spanwise coordinate [m].

Greek symbol

ρ	air density [$kg m^{-3}$].

Subscripts

b	bulk mean
N	rib index
s	smooth
w	wall.

flow and heat transfer studies were previously performed with only a single detached square rib [13,14]. The present study thus focuses on the turbulent heat transfer and friction in a rectangular duct with a detached square-rib array, and to fulfill the following objectives:

(1) The hot spots existing behind the attached solid ribs deteriorate duct materials. One of the purposes in the present paper is to examine whether the proposed detached square-rib array can effectively eliminate the hot spots, as the flow proceeds from developing to spatially periodic state.

(2) Thermal performance comparison between detached-ribbed, attached-ribbed and smooth ducts are performed in this study to determine the merits in using a detached-rib array.

(3) Semi-empirical correlations of fully developed heat transfer and friction in terms of Reynolds number are developed in the present paper for a duct with detached ribs. Such correlations have not been proposed in the past for ducts with a detached-rib array, and may be helpful for the design of related devices such as compact heat exchangers and internal cooling passages of the turbine blades.

(4) The configurations of the internal cooling passages of the turbine blades are usually very short, typically 10–15 times hydraulic diameter, and started with a nearly abrupt-contraction entrance. The effect of thermal entry length on the length mean Nusselt number ratio may thus be significant, which, however, has not been studied in the past for the detached-ribbed ducts, and is investigated in the present work.

EXPERIMENTAL PROGRAM

Flow system

The flow system, test section and LHI experimental setup are shown in Fig. 1. The open-loop flow circuit was operated in the suction mode and oriented horizontally. Air was drawn into the test section from the temperature-controlled laboratory room. After traversing the test section, the air flowed subsequently through a flow straightener, a rotameter and a bellows, and then was exhausted by a 3 h.p. blower.

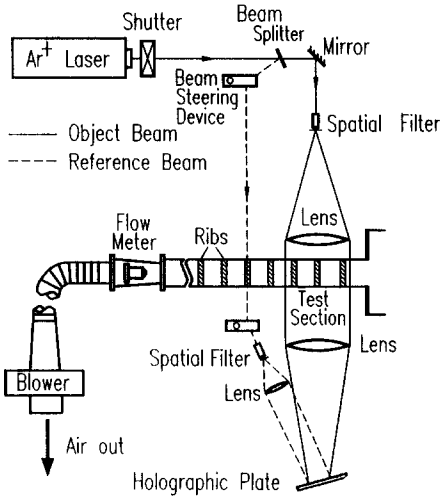

Fig. 1. Schematic drawing of flow system, test section, and LHI setup.

The blower was situated in a service corridor outside the laboratory to insulate the vibration, and its discharge (heated air) was vented outside the building. The upstream end of the test section was connected with a plexiglass plenum, which ensured the air entering the test duct had an abrupt-contraction-entrance condition. The contraction area ratio between the plenum and the test duct was 11.25. This inlet condition was arbitrarily selected [15] to simulate turbine cooling channels because the actual turbine cooling channels may have a wide range of inlet configurations, which depend on the specific design.

LHI system

In the present work the flow field temperature distribution was measured by a real-time LHI whose optical circuit (Fig. 1) and experimental procedure were described in detail by Liou and Hwang [4]. Please refer to this earlier paper for more detail. It is noteworthy that a combination of a holographic film plate holder and a liquid gate was used to provide in-place development of film plate as required for subsequent real-time work. The photographic emulsion 8E56, made by Agfa-Gevaert Ltd, was found to be a suitable material for the present work. Through a CCD camera, the instantaneous interference field was monitored on a multisync monitor and recorded on a VHS videocassette recorder for storage and further image processing.

Test section and instruments

The configuration, coordinate system, and dimensions of the test duct and the associated plenum are sketched in Fig. 2. The test duct, consisting of two principal walls (the top and bottom walls of the duct) and two side walls, was 1600 mm long and had a rectangular cross-section 160×40 mm^2 (Y–Z plane), i.e. an aspect ratio of 4:1. The bottom principal wall, fabricated from a highly polished stainless steel plate of 0.3 mm thickness, was covered by sharp-edged aluminum ribs of size 5.2×5.2 mm^2. A thermofoil of thickness 0.18 mm emits heat to the bottom wall of the test section. The thermofoil was adhered uniformly between the stainless steel plate and bakelite plate and could be controlled individually by a 60 W d.c. power supply for controllable electrical heating to the test section. Additionally, the heated plate was insulated by 30-mm-thick bakelite wood to prevent heat loss. The side walls of the entire heated test duct were made of plexiglass plates to provide optical access for LHI measurements. The construction of the detached-ribbed wall is displayed in detail in Fig. 2.

As shown in Fig. 2, the interferograms were taken for the regions of $0 \leqslant X/H \leqslant 21$, $18 \leqslant X/H \leqslant 41$, $38 \leqslant X/H \leqslant 61$, and $148 \leqslant X/H \leqslant 171$, respectively. The first three were situated in the developing region and the last one was situated in the fully developed region. It was one rib pitch (Pi) from the duct entrance to the first rib. The entire test section was mounted on a modified milling machine with four vibration-isolation mounts to allow vertical and horizontal movement, and hence successive scanning of the expanded object beam. Additionally, for wall temperature measurements the regions corresponding to the interferometric measurements were instrumented with 90 copper–constantan thermocouples (60 for the developing region and 30 for the fully developed region) distributed along the centerline ($Z = 0$) of the heated plate. The junctions 0.2 mm in a diameter were cemented into small holes drilled into the back side of the heated plate, approx. 1.0 mm from the front surface. A Yokogawa DA-2500 hybrid recorder and a PC-AT were used for temperature readings and recordings.

The measurements of centerline pressure distributions for the developing flows were carried out by a Pitot tube, which was inserted from the side wall of the test duct to transverse across and along the flow direction. Also, five pressure taps were used for static pressure drop measurements across the fully developed region of the test duct. The pressure taps were drilled at intervals of 10.4 cm, with the first tap 45 cm from the duct inlet. The pressure drop of the present study was based on the adiabatic conditions. To measure static pressure, a microdifferential transducer (Kyowa, PDL-40B, $\pm 0.1\%$) was connected to each pressure tap on the duct wall. The measured pressure signal was subsequently amplified by a Kyowa WGA-200A amplifier and read from a digital readout.

Experimental conditions

The Reynolds number (Re), based on the duct hydraulic diameter (64 mm) and bulk mean velocity, extended from 5.0×10^3 to 5.0×10^4; while the rib angle of attack, the ratio of rib pitch to height (Pi/H), the rib to duct height ratio ($H/2B$), and the non-dimensional distance between the detached ribs and duct wall (C/H) were 90°, 10, 0.13 and 0.58, respec-

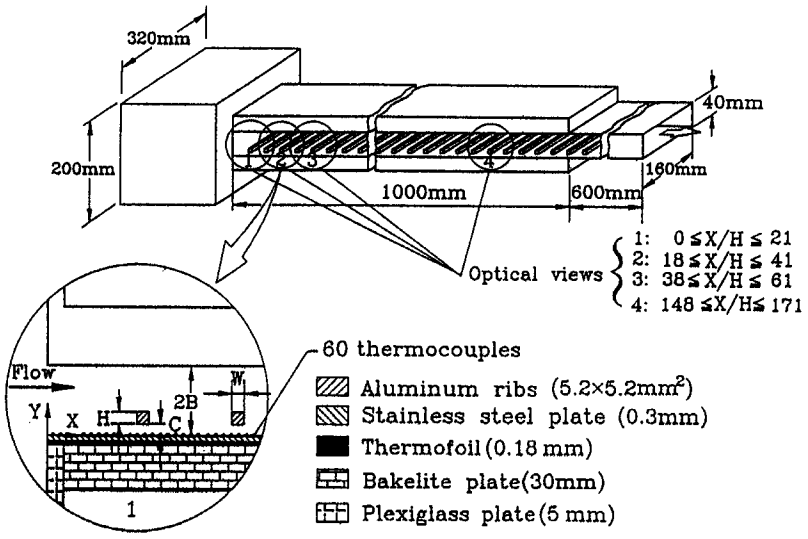

Fig. 2. Sketch of configuration, coordinate system and dimensions of the test section.

tively. $C/H = 0.58$ was chosen in this study because at about this value the heat transfer augmentation was most effective for fluid flows around a circular cylinder near a plane, as reported by Marumo *et al.*[16].

Data analysis and uncertainty

The distributions of the centerline pressure drop for the developing ribbed-duct flows are non-dimensionalized by the fluid dynamic pressure as

$$C_f = (P_X - P_0)/(\rho U^2/2) \quad (1)$$

and the friction factor in the fully developed region is expressed as

$$f = -(\mathrm{d}P/\mathrm{d}X)D_e/(\rho U^2/2). \quad (2)$$

Note that the variance of pressure difference in the duct spanwise (Z) and transverse (Y) directions is very slight (about 6% in scatter). This observation coincides with that pointed out by Han *et al.* [1], which states that the pressure difference is almost the same when measured from the pressure taps, either on the ribbed wall or on the smooth side wall. $\mathrm{d}P/\mathrm{d}X$ is evaluated by taking the ratio of the pressure difference ΔP between corresponding points (pressure taps) of successive cycles and the rib pitch. The maximum uncertainties of C_f and f are estimated to be less than 6.2 and 7.3%, respectively. The entire investigated temperature field is revealed by infinite-fringe interferometry, which enables the calculations of local and average heat transfer coefficients to be made [17]. The significant errors of the interferometry usually encountered are the end effect and the refraction effect errors. By using the interferometry error analysis suggested in Goldstein [18], it is found that the resulting errors in the fringe shift due to the end and refraction effects are about 6 and 4%, respectively. The convection heat transfer coefficient of the heated wall can be presented in terms of the local Nusselt number Nu, which is defined as

$$Nu = h \cdot D_e/k_f = -(\mathrm{d}T/\mathrm{d}Y)_w \cdot D_e/(T_w - T_b) \quad (3)$$

where $(\mathrm{d}T/\mathrm{d}Y)_w$ is determined by curve fitting, based on a least-squares method through the near-wall values for temperature and fringe shift; T_w is read from the thermocouple output; and T_b is calculated from an energy balance, $T_b = T_{in} + Q/(m \cdot c_p)$, where Q is the quantity of heat given to air from entrance to the considered cross-section of the duct and can be obtained by the integrated form of

$$\int_0^X [k_f \cdot (\mathrm{d}T/\mathrm{d}Y)_w \cdot 2A] \cdot \mathrm{d}X.$$

.The maximum uncertainty of the local Nusselt number is estimated to be less than 6.5% by the uncertainty estimation method of Kline and McClintock [19]. The average Nusselt number for the periodically fully developed region is evaluated by the following equation:

$$\overline{Nu}_p = q_{conv} \cdot D_e/[k_f \cdot (\bar{T}_w - \bar{T}_b)]$$

$$= D_e \cdot \int_0^{L_h} (\mathrm{d}T/\mathrm{d}Y)_w \cdot \mathrm{d}x/[L_h \cdot (\bar{T}_w - \bar{T}_b)] \quad (4)$$

where q_{conv} is the convective heat flux from the wall and can be estimated by interferometry or subtracting the heat loss from the supplied electrical input. $\bar{T}_w$ is the average wall temperature in one rib pitch, $\bar{T}_b$ is the average bulk mean temperature of air, and L_h is the wetted length of heated surface in one pitch. Thermal conductive loss along the flow direction near the start and the end of heating and from the insulation material (bakelite wood) of the top and bottom heated plates is estimated by measuring the wall temperatures and assuming one-dimensional heat flow, and is found

to be 0.6 and 12.9%, respectively. Heat loss from the side walls (plexiglass) of the flow passage material is also calculated by applying the natural convection between them and atmosphere, and is about 4.1%. The maximum uncertainty of $\overline{Nu}_p$ is estimated to be less than 9.8%. The local and average Nusselt numbers of the present study are normalized by the Nusselt number for fully developed turbulent flow in smooth circular tubes, correlated by Dittus and Boelter as

$$Nu/\overline{Nu}_s = Nu/(0.023 \cdot Re^{0.8} \cdot Pr^{0.4}). \quad (5)$$

RESULTS AND DISCUSSION

Skin-friction coefficient

The streamwise evolution of the centerline pressure coefficient is depicted in Fig. 3, where the previous results for the case of the attached ribs are also included for qualitative comparison. For a duct with periodic ribs the flow is considered to be fully developed, as the flow pattern in a pitch repeats itself pitch-by-pitch [20]. Similarly, the pressure has certain periodic characteristics in the fully developed region, that is, the pressure differences between X_1 and X_1+Pi, X_1+Pi and X_1+2Pi, X_1+2Pi and X_1+3Pi,.... etc. are identical. In other words, if the pressures at points X_1, X_1+Pi, X_1+2Pi, X_1+3Pi,... are plotted, they will fall on a straight line, as shown in Fig. 3. It is seen that the hydrodynamic development length is about $x/D_e = 3$, which is equivalent to that reported for the attached ribbed duct flow [5, 15]. Downstream of a hydrodynamic development length, the streamwise pressure distribution within a given pitch is not linear: however the whole distribution repeats pitch-by-pitch.

Isotherm contours

Typical examples of real-time interferograms taken from the temperature fields of the present duct flow with a rib array placed a small distance from the heated wall are shown in Figs. 4 and 5. The interferogram in Fig. 4(a) clearly shows the thermal boundary layer development from the duct inlet [left end in Fig. 4(a)]. Near the inlet ($X/H = 0$), the reattachment ($X/H \approx 4$) on the wall of the interference fringe which is the closest to the heated wall indicates flow separation at the abrupt-contraction inlet, formation of the vena contracta, and flow reattachment on the wall. A similar behavior, but more pronounced, was also observed previously by Liou and Hwang [5] for the developing duct flow with attached rib arrays on two opposite walls. The thermal boundary layer development is disturbed by the presence of the detached-rib array, as evidenced by the distortion of fringes around the rib top and bottom. The disturbance occurs pitch-by-pitch and Fig. 4(b) provides an example, showing periodic repeat of the inter-rib interferogram for $12.0 \leqslant X/D_e \leqslant 13.9$.

A closer look of the interference fringe distributions around the first four detached ribs is given in Fig. 5(a)–(d). Typical temperature steps associated with each fringe shift at $X_N/H = 0.5$ in Fig. 5(d) are listed in Table 1. It is seen that the temperature gradient near the heated wall is significantly steeper than that near the rib's front face or rear face, as evidenced by the relatively clustered thin fringes near the heated wall. In addition, the near-wall fringe number increases with increasing rib index. More specifically, the number of fringes in the region to the right of the detached rib and near the heated wall increases from three for the first rib to five for the fourth rib, a phenomenon not observed for the duct flow with attached ribs. Also note that the temperature distribution around each rib downstream of the third

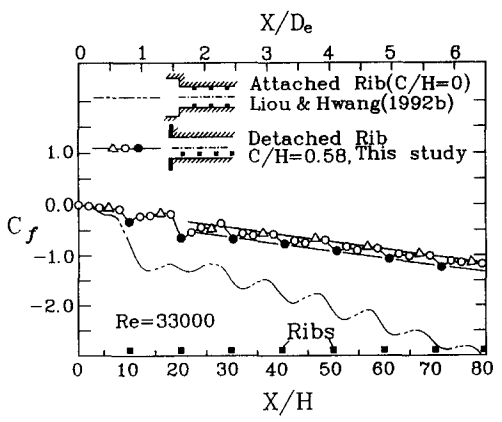

Fig. 3. Measured centerline pressure coefficient distribution for $Pi/H = 10$.

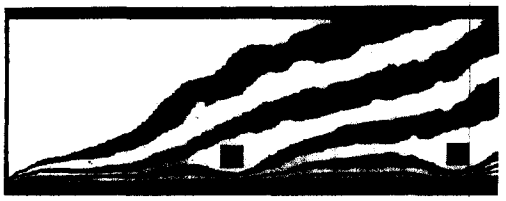

(a) Re = 12600, Pi/H = 10, $0 \leqq X/D_e \leqq 2.0$, C/H = 0.58 (View1)

(b) Re = 12600, Pi/H = 10, $12 \leqq X/D_e \leqq 13.9$, C/H = 0.58 (View4)

Fig. 4. Examples of LHI of developing and periodic fully developed duct flows with a detached-rib array.

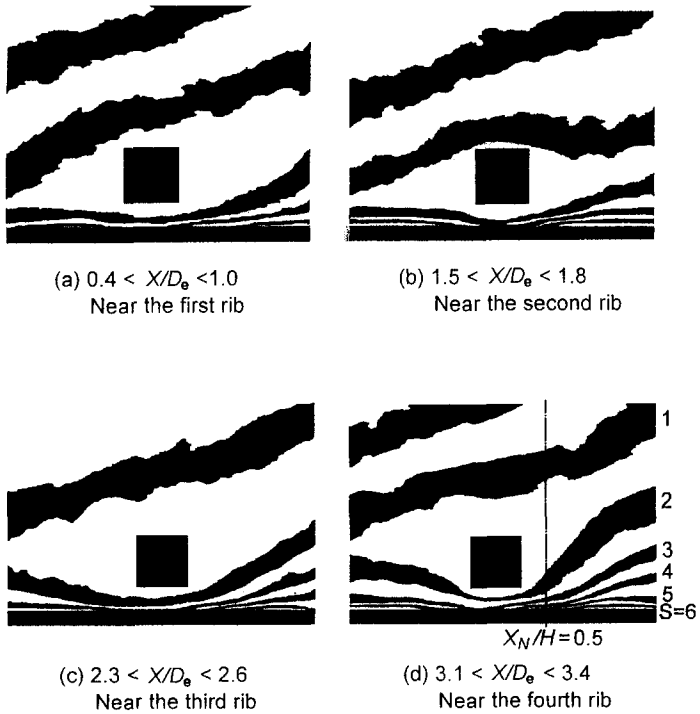

Fig. 5. Interferograms around the first four ribs for $Re = 12\,600$ and $C/H = 0.58$.

rib remains invariant pitch-by-pitch, since beyond the third rib the flow attains thermal fully developed, as will be shown shortly in terms of local Nusselt number distribution. In other words, displacing the rib array a small distance from the heated wall has the advantage of allowing the heat transfer rate in the region near the wall and to the right of the rib to be increased with increasing rib index up to the fully developed value at the fourth rib and then remain so downstream, a feature lacking in the attached-ribbed duct where the heat transfer rate in the rear concave corner of the rib deteriorates significantly [4, 21].

Local Nusselt number

The local Nusselt number of the heated wall can be obtained from the above interferograms and wall temperature measurements and the results are shown in Fig. 6 for Reynolds numbers of 1.26×10^4 and 3.3×10^4. The previous results for a smooth duct with a sharp entrance [5, 22] are also plotted as Fig. 6(a) for comparison. In the upstream portion of the first rib, Fig. 6(b) depicts that the general behavior of the two curves affected by the abrupt inlet contraction for the ribbed duct flows is similar to that of the entrance region of a smooth duct, namely, large heat transfer coefficient near the leading edge of the duct inlet due

Table 1. Temperature differences associated with each fringe shift derived from cutout region in Fig. 5(d)

ΔS (fringe shift)	Y [mm]	ΔT [°C]
6	2.715	4.31
5	4.828	4.21
4	5.664	4.09
3	6.277	3.99
2	7.057	3.90
1	10.029	

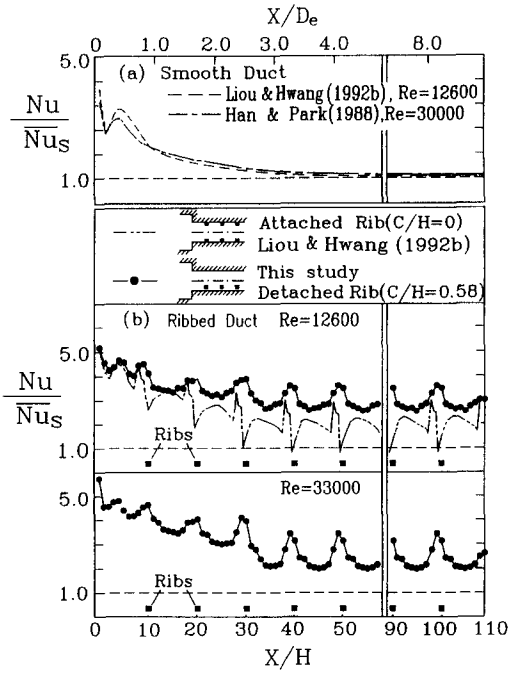

Fig. 6. Local Nusselt number ratio vs X/H in smooth and detached-ribbed ducts.

to the large temperature gradient near the leading edge of the duct inlet (Fig. 5a) and the formation of the second peak value of $Nu/\overline{Nu}_s$ by the impingement of the reattaching flow from the duct inlet on the duct wall. The growth of thermal boundary layer and resulting decrease in temperature difference between the core fluids and heated wall are responsible for the subsequent decrease of $Nu/\overline{Nu}_s$ approaching the fully developed value for the smooth duct flow, while for the duct flow with a detached-rib array $Nu/\overline{Nu}_s$ decreases slowly with increasing distance, setting into a periodic pattern after the first three ribs or about $X/D_e = 3$ ($X/H = 37$). Similar trends were observed by Han [15] and Liou and Hwang [5] for the duct flows with attached ribs. However, a significant difference in the level of $Nu/\overline{Nu}_s$ between the detached- and attached-ribbed duct flow is clearly revealed by Fig. 6(b). Regions where $Nu/\overline{Nu}_s < 1$ for the duct being cooled from the inside are often called hot spots and appear in the attached-ribbed duct flow after the third pair of ribs (about $X/D_e = 3$ or $X/H = 40$). In contrast, the hot spots occurring around the rib's rear corners formed by the intersection of ribs and duct wall do not arise in the present detached-ribbed duct. In other words, an improvement of the local heat transfer distribution is achieved by detaching a rib array a small distance from the heated wall and in turn eliminating the nearly stagnant low-speed recirculating fluids in the rib's rear concave corners. Quantitatively, the level of heat transfer enhancement attained in this study is about 1.8–5.8 times $\overline{Nu}_s$ for the Reynolds number range investigated.

Average friction and heat transfer

From the foregoing presented results, the Reynolds number dependence of average friction factor and Nusselt number for fully developed region ($X/H > 40$) can be obtained and plotted in Fig. 7 where the corresponding results of smooth ducts and attached-ribbed ducts [23] are also included for comparison. As expected, the average Nusselt number increases with increasing Reynolds number, whereas the average friction factor decreases with increasing Reynolds number. These trends can be correlated by the following power law for Reynolds number range of 5×10^3–5×10^4:

$$f = 5.979 \cdot Re^{-0.363} \tag{6}$$

$$\overline{Nu}_p = 0.364 \cdot Re^{0.604}. \tag{7}$$

The maximum deviations of the measured data from the above correlations are 3.9 and 5.2%, respectively, for the average friction factor and Nusselt number. Figure 7 further shows that the extent of increased toll in f for the present detached-ribbed duct flow is a factor of 5.45–7.45 and 1.57–1.93, respectively, as compared with those of the smooth-duct flow and attached-ribbed duct flow, while the level of heat transfer enhancement is approx. 1.95–3.03 and 1.21–1.30, respectively, for the test range of Re.

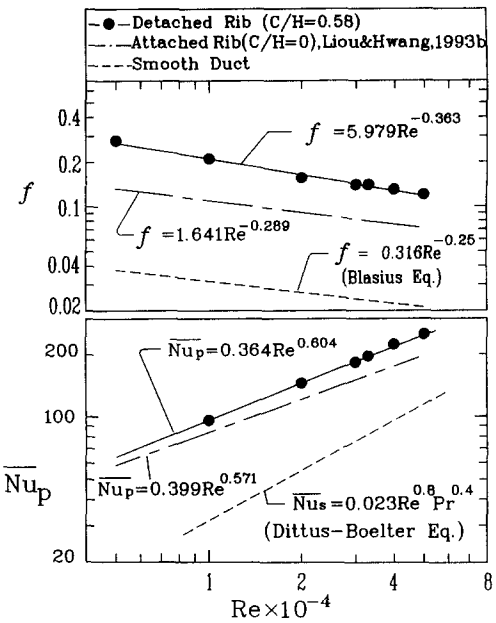

Fig. 7. Average Nusselt number and friction factor vs Re for $Pi/H = 10$.

Owing to the opposite trends in the Reynolds number dependence of the average friction factor and Nusselt number, performance analyses are necessary for knowing the net benefit of using a periodically detached-ribbed duct instead of a smooth one or an attached-ribbed duct, and are reported below.

Performance analysis

Two types of heat transfer performance, equal mass flow rate and equal pumping rate constraints, are undertaken. In order to impose the constraint of equal pumping power, it is necessary to find the relationship between the Reynolds number relative to the ribbed duct (Re) and the corresponding Reynolds number for the smooth duct (Re^*) that yields the same pumping power. The relation between Re and Re^* has been given by Liou and Hwang [5] and is in the form

$$Re^* = f^{1/3} \cdot Re \cdot [0.316 \cdot (Re^*)^{-0.25}]^{-1/3}. \tag{8}$$

The results obtained from the solution of equation (8) are presented in Fig. 8(a). As expected, ribbed ducts have to be operated at a lower Reynolds number than smooth ducts in order to achieve equal pumping power. The new result is that for ribbed ducts the detached-ribbed duct has to be operated at a lower Reynolds number than the attached-ribbed duct in order to achieve equal pumping power. The reason is that the flow separates at the top and bottom surfaces of the detached ribs, whereas the flow separates only at the top surface of the attached ribs.

With Re^* and Re information from Fig. 8(a), the corresponding Nusselt numbers of smooth ducts can be evaluated, and then the ratios $\overline{Nu}_p/\overline{Nu}_s$ with $\overline{Nu}_s$ corresponding to Re and $\overline{Nu}_p/\overline{Nu}_s^*$ with $\overline{Nu}_s^*$ corresponding to Re^* determined and plotted in Fig.

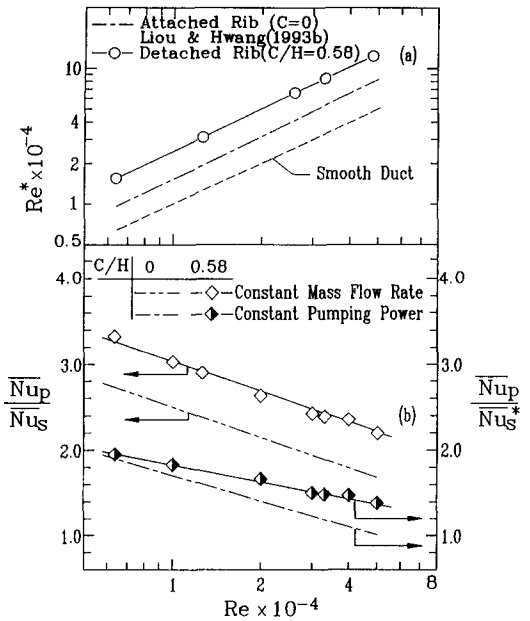

Fig. 8. (a) Relationship between Re for ribbed ducts and Re^* for smooth ducts (equal pumping power constraint); (b) comparison of constant mass-flow-rate and constant-pumping-power fully developed heat transfer coefficients for the ribbed and smooth ducts ($Pi/H = 10$).

8(b). It is seen that $\overline{Nu}_p/\overline{Nu}_s$ for the case of equal mass flow rate is much higher than $\overline{Nu}_p/\overline{Nu}_s^*$ for the case of equal pumping power, the factor ranging from 1.6 to 1.7 for the detached-ribbed duct. More importantly, regardless of the set of constraints employed, the improvement in Nusselt number ratios of the detached-ribbed/attached-rib duct is more pronounced at low Reynolds numbers than at high Reynolds numbers, the factors ranging from 2.2 to 3.3/1.7 to 2.7 and 1.4 to 2.0/1.0 to 1.9 for the constraints of equal mass flow rate and equal pumping power, respectively. Further, for the Reynolds number range tested, heat transfer augmentation by detaching a rib array a small distance of $C/H = 0.58$ from the heated wall is about factors of 1.2–1.3 and 1.1–1.4 higher than by attaching a rib array onto the heated wall ($C/H = 0$) for the constraints of equal mass flow rate and equal pumping power, respectively.

Length mean Nusselt number

For a typical internal cooling passage of turbine blades, because the first pass of the ribbed ducts is about 10–15 hydraulic diameters in length with an abrupt-contraction inlet, the effect of the entry length could be significant and is worth investigation. It is appropriate, but has been seldom addressed in the past, to characterize the entry-length effect in terms of a length mean Nusselt number. As presented before, the local Nusselt number ratios maintain the same periodic distribution after $X/D_e \geqslant 3$. Thus, for ducts with lengths greater than the entry length, it should be possible to express the length mean Nusselt number in the form

$$\overline{Nu}_m = [3D_e \cdot \overline{Nu}_d + (X - 3D_e) \cdot \overline{Nu}_p]/X \quad (9)$$

where $\overline{Nu}_d$ is the mean Nusselt number obtained by integrating Nu from $X = 0$ to $X = 3D_e$ and $\overline{Nu}_p$ is the pitch-averaged Nusselt number in the fully developed region. In combining $\overline{Nu}_p$ correlated by equation (7) and $\overline{Nu}_d$, equation (9) becomes

$$\overline{Nu}_m/\overline{Nu}_p = 1 + 3 \cdot (\overline{Nu}_d/\overline{Nu}_p^{-1})/(X/D_e). \quad (10)$$

In general, $\overline{Nu}_d/\overline{Nu}_p$ in equation (10) is a function of Prandtl number, Reynolds number and detached distance [5]. For the present study equation (10) can be reduced to

$$Re = 12\,600 \quad \overline{Nu}_m/\overline{Nu}_p = 1 + 1.06/(X/D_e)$$
$$Re = 33\,000 \quad \overline{Nu}_m/\overline{Nu}_p = 1 + 0.79/(X/D_e) \quad (11)$$

and is plotted in Fig. 9, where the results of the smooth ducts with nozzle-like [24] and abrupt-contraction entrance [25] and the attached-ribbed duct are also included for comparison. As one can see from Fig. 9, the effect of the abrupt-contraction entrance of the detached ribbed duct on the length mean Nusselt number ratio is the least substantial, whereas the smooth duct is the most, among the duct flows with the same inlet condition. The reason is given below. The mechanism that is responsible for large heat transfer coefficients near the abrupt-contraction inlet of the duct, i.e. flow separation, recirculation and redevelopment, occurs everywhere throughout the ribbed ducts due to the presence of the periodic turbulence promoters. Therefore, the magnitude of $\overline{Nu}_p$ is comparable to the values of $\overline{Nu}_d$ in the developing region near the duct inlet. Thus, the levels of length mean Nusselt number ratio distribution of the ribbed ducts with an abrupt-contraction entrance, which are normalized by the asymptotic value $\overline{Nu}_p$, are much lower

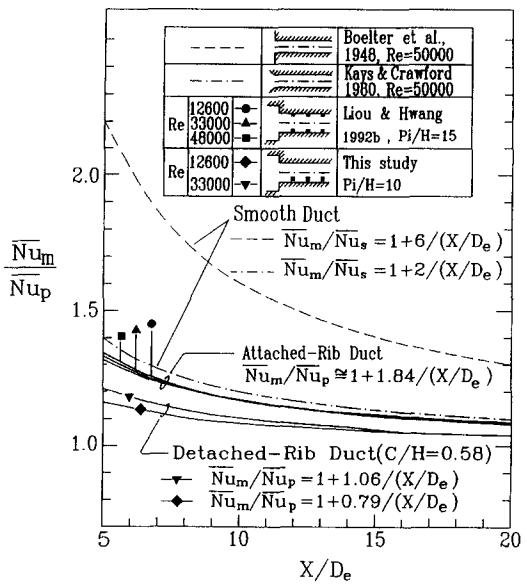

Fig. 9. Effect of Re on the length mean Nusselt number distribution for ribbed and smooth ducts.

than that of the smooth duct with an abrupt-contraction entrance and closer to that of the smooth duct with a nozzle-like entrance [26], as shown in Fig. 9. Moreover, from the foregoing sections, the $\overline{Nu}_p$ level for the case of the detached-ribbed duct flow is higher than for the case of the attached-ribbed duct flow, as shown in Fig. 7; however, the difference in the levels of $\overline{Nu}_d$ between the two cases in the developing region near the duct entrance is not so large as that in the levels of $\overline{Nu}_p$ in the fully developed region. Consequently, Fig. 9 reveals that $\overline{Nu}_m/\overline{Nu}_p$ distribution for the detached-ribbed duct flow is lower than for the attached-ribbed duct flow. Quantitatively, for square-ribbed ducts of 10–15 hydraulic diameters in length with an abrupt-contraction inlet, the length mean Nusselt numbers are 5.3–10.6 and 12–18% above the corresponding asymptotic values for the detached- and attached-ribbed duct flows, respectively. That is, the entry length effects are 5.3–10.6 and 12–18%, respectively, for the detached- and attached-ribbed duct flows.

SUMMARY AND CONCLUSIONS

The following conclusions can be drawn from the data presented:

(1) The developing flow in the present detached square-ribbed duct is found to become hydrodynamically and thermally fully developed after the first three ribs or $X/D_e > 3$, a result similar to that in the attached-ribbed duct flows.

(2) The heat transfer deterioration occurring behind the attached solid ribs is effectively removed by adopting the detached-rib array. However, the detached-ribbed duct has to be operated at a lower Reynolds number than the attached-ribbed duct in order to achieve equal pumping power.

(3) For the Reynolds number range tested, heat transfer augmentation by detaching a square-rib array a small distance of $C/H = 0.58$ from the heated wall is about a factor of 1.2–1.3 and 1.1–1.4 higher, respectively, than by attaching the rib array onto the heated wall ($C/H = 0$) for the constraints of equal mass flow rate and equal pumping power.

(4) For square-ribbed ducts of 10–15 hydraulic diameters in length with an abrupt-contraction inlet, the length mean Nusselt numbers are 5.3–10.6 and 12–18% above the corresponding asymptotic values for the detached- and attached-ribbed duct flows, respectively.

(5) Correlations for heat transfer and friction in the periodic fully developed region and length mean Nusselt number ratio are developed.

Acknowledgement— Support for this work was provided by the National Science Council of the Republic of China under contract No. NSC82-0401-E007-289.

REFERENCES

1. J. C. Han, J. S. Park and C. K. Lei, Heat transfer enhancement in channels with turbulence promoters, *Trans. ASME J. Engng Gas Turbines Pwr* **107,** 628–635 (1985).
2. D. E. Metzger, C. S. Fan and Y. Yu, Effects of rib angle and orientation on local heat transfer in square channels with angled roughness ribs. In *Compact Heat Exchangers, a Festschrift for A. L. London*. Hemisphere, Washington, DC (1990).
3. A. E. Bergles, Some perspectives on enhanced heat transfer–second-generation heat transfer technology, *Trans. ASME J. Heat Transfer* **110,** 1082–1096 (1988).
4. T. M. Liou and J. J. Hwang, Turbulent heat transfer augmentation and friction in periodic fully developed channel flows, *Trans. ASME J. Heat Transfer* **114,** 56–64 (1992).
5. T. M. Liou and J. J. Hwang, Developing heat transfer and friction in a ribbed rectangular duct with flow separation at inlet, *Trans. ASME J. Heat Transfer* **114,** 565–573 (1992).
6. T. M. Liou, Y. Y. Wu and Y. Chang, LDV measurements of periodic fully developed main and secondary flows in a channel with rib-disturbed walls, *Trans. ASME J. Fluids Engng* **115,** 109–114 (1993).
7. J. J. Hwang and T. M. Liou, Augmented heat transfer in a rectangular channel with permeable ribs mounted on the wall, *Trans. ASME J. Heat Transfer* **116,** 890–897 (1994).
8. H. Fujita, H. Takahama and R. Yamashita, Forced convection heat transfer on a plate with a cylinder inserted in the boundary layer, *Heat Transfer—Jap. Res.* **7,** 69–78 (1978).
9. Y. Kawaguchi, K. Suzuki and T. Sato, Heat transfer promotion with a cylinder array located near the wall, *Int. J. Heat Fluid Flow* **6,** 249–255 (1985).
10. K. Oyakawa, T. Shinzato and I. Mabuchi, Effect on heat transfer augmentation of some geometric shapes of a turbulence promoter in a rectangular duct, *Bull. JSME* **29,** 3415–3420 (1986).
11. M. Yao, M. Nakatani and K. Suzuki, An experimental study on pressure drop and heat transfer in a duct with a staggered array of cylinders. In *Proceedings of ASME–JSME Thermal Engineering Joint Conference* (Edited by P. J. Marto and I. Tanasawa), Vol. 5, pp. 189–196. American Society of Mechanical Engineers (1987).
12. M. Yao, M. Nakatani and K. Suzuki, Flow visualization and heat transfer experiments in a duct with a staggered array of cylinders. *Exp. Thermal Fluid Sci.* **2,** 193–200 (1989).
13. H. Suzuki, Y. Inoue, T. Nishimura, K. Fukutani and K. Suzuki, Unsteady flow in a channel obstructed by a square rod (crisscross motion of vortex), *Int. J. Heat Fluid Flow* **14,** 2–9 (1993).
14. H. Suzuki, K. Fukutani, T. Takishita and K. Suzuki, Flow and heat transfer characteristics in a channel obstructed by a square rod mounted in asymmetric positions, *Proceedings of the 6th International Symposium on Transport Phenomena in Thermal Engineering*, pp. 353–358. Seoul, Korea. Hemisphere Publishing Corporation (1993).
15. J. C. Han, Heat transfer and friction characteristics in rectangular channels with rib turbulators, *Trans. ASME J. Heat Transfer* **110,** 321–328 (1988).
16. E. Marumo, K. Suzuki and T. Sato, Turbulent heat transfer in a flat plate boundary layer disturbed by a cylinder, *Int. J. Heat Fluid Flow* **6,** 241–248 (1985).
17. W. Hauf and U. Grigull, Optical methods in heat transfer. In *Advances in Heat Transfer* (Edited by J. P. Hartnett and T. F. Irvine, Jr), Vol. 6, pp. 133–136. Academic Press, New York (1970).
18. R. J. Goldstein, Optical measurement of temperature. In *Measurements in Heat Transfer* (Edited by E. R. G.

Eckert and R. J. Goldstein) (2nd Edn), pp. 241–294. Hemisphere, Washington, DC (1976).
19. S. J. Kline and F. A. McClintock, Describing uncertainties on single-sample experiments, *Mech. Engng* **57**, 3–8 (1953).
20. T. M. Liou and J. Lin, Measurements of turbulent flow in a duct with repeated ribs applied to two opposite walls, *J. Chin. Inst. Engrs* **11** (4), 319–326 (1988).
21. J. F. Lockett and M. W. Collins, Holographic interferometry applied to rib-roughness heat transfer in turbulent flow, *Int. J. Heat Mass Transfer* **33**, 2439–2449 (1990).
22. J. C. Han and J. S. Park, Developing heat transfer in rectangular channels with rib turbulators, *Int. J. Heat Mass Transfer* **31**, 183–195 (1988).
23. T. M. Liou, J. J. Hwang and S. H. Chen, Simulation and measurement of enhanced turbulent heat transfer in a channel with periodic ribs on one principal wall, *Int. J. Heat Mass Transfer* **36**, 507–517 (1993).
24. C. A. Sleicher and M. Tribus, *J. Heat Transfer Fluid Mech. Inst.*, Stanford, CA, p. 59 (1956). Data reported by Kays and Crawford. In *Convective Heat and Mass Transfer* (2nd Edn), p. 264. McGraw-Hill, New York (1980).
25. L. M. K. Boelter, G. Young and H. W. Iversen, An investigation of aircraft heaters—distribution of heat-transfer rate in the entrance section of a circular tube, NACA Technical Note No. 1451 (1948). Data reported by Kays and Crawford. In *Convective Heat and Mass Transfer* (2nd Edn), p. 269. McGraw-Hill, New York (1980).
26. W. M. Kays and M. E. Crawford, *Convective Heat and Mass Transfer* (2nd Edn). McGraw-Hill, New York (1980).